JOURNAL OF MATERIALS SCIENCE 21 (1986) 2289–2296

Electrical transport in heavy rare-earth vanadates

KANCHAN GAUR, H. B. LAL
Department of Physics, University of Gorakhpur, Gorakhpur 273001, India

This paper reports measurements of electrical conductivity (σ) and Seebeck coefficient (S) between 300 and 1250 K and differential thermal analysis (DTA) and thermogravimetric analysis (TGA) between 300 and 1200 K, together with X-ray diffraction studies of heavy rare-earth vanadates (RVO_4 with R = Tb, Dy, Ho, Er and Yb). All these vanadates have been found to have a tetragonal unit cell. The DTA study shows a flat dip in the temperature interval 1075 to 1300 K, indicating a possible structural phase transition of these compounds. Practically no weight loss has been observed in TGA from 300 to 1200 K in any of the vanadates. All RVO_4 are semiconducting materials with the room-temperature σ value lying in the range 10^{-12} to $10^{-3}\,\Omega^{-1}\,m^{-1}$, becoming of the order of $10^{-2}\,\Omega^{-1}\,m^{-1}$ around 1000 K. The electrical conductivity of all vanadates exhibits an exponential increase in the temperature intervals 420 K to T_1 and T_1 to T_2, with different values of the activation energy. A $\log\sigma$ against T^{-1} plot shows a peak around T_3 and drops to a minimum value around T_4, before increasing again with temperature. $T_4 > T_3 > T_2 > T_1$ are different for different vanadates and these are termed "break temperatures". T_4 lies well within the temperature range of the DTA peak and can be termed the phase transition temperature. In the lower temperature interval the electrical conduction is essentially extrinsic. The localized charge carriers on defect centres conduct by a hopping mechanism. The defect centres are V^{4+} ions in all vanadates with R^{4+} centres in some of them. It is concluded that in the temperature interval $T_1 < T < T_2$ the conduction mechanism is of the intrinsic band type, with oxygen 2p and vanadium 3d as the valence and conduction bands, respectively. Related parameters like the energy band gap and the mobilities of the charge carriers have also been evaluated. The low values of mobility suggest that large polarons with intermediate coupling are the charge carriers rather than bare electrons in the intrinsic region. All these vanadates tend to become metallic, but before this is achieved the phase change makes the conductivity smaller.

1. Introduction

Mixed oxides of rare-earth and iron group elements are well known for their wide-ranging physical properties. Among them vanadates of the rare earths (RVO_4, R standing for lanthanum to lutetium) form a group of compounds revealing interesting structural and magnetic transformations [1]. We have recently reported the unusual magnetic behaviour of gadolinium [2], light [3] and heavy [4] rare-earth vanadates at higher temperatures, and the electrical transport and semiconductor–semimetal transition in $LaVO_4$ [5]. The interesting and to some extent unusual behaviour of these compounds prompted us to investigate the electrical transport properties of the whole series of rare-earth vanadates. As a part of this plan we have already studied and reported the electrical transport properties of light rare-earth vanadates [6]. This paper reports the electrical transport properties of heavy rare-earth (R = Tb, Dy, Ho, Er and Yb) vanadates. All these vanadates have a tetragonal unit cell with cell parameters as given in Table I at room temperature [7].

2. Material preparation and experimental techniques

The details of the preparation of all rare-earth vanadates, including starting materials, have already been reported in our earlier publications [2–5]. For characterization the X-ray diffraction patterns were recorded using powdered samples employing Cu$K\alpha$ (λ = 0.15405 nm) radiation, and the evaluated unit cell parameters were almost the same as those given in Table I. Differential thermal analysis (DTA) and thermogravimetric analysis (TGA) studies were performed at a heating rate of $10^\circ\,C\,min^{-1}$. The electrical conductivity (σ) and Seebeck coefficient (S) were measured using sample holders and procedures as described in several publications of our group [8–11].

3. Results

Measurements of σ and S were performed on pressed pellets because of the difficulty of growing the large single crystals of these compounds needed for such measurements, due to their high melting point and our limited facilities. In pellets, grain boundaries and air

0022–2461/86 $03.00 + .12

TABLE I Unit cell parameters of RVO_4 at 398 K (tetragonal unit cell)*

R	Unit cell parameters (nm)		Bond distances (nm)		
			R–O	R–O	V–O
	a	*c*			
Ce	0.7399	0.6496	0.254	0.243	0.172
Pr	0.7367	0.6468	0.253	0.241	0.172
Nd	0.7329	0.6436	0.252	0.240	0.172
Sm	0.7266	0.6394	0.249	0.238	0.172
Eu	0.7237	0.6368	0.248	0.235	0.172
Gd	0.7211	0.6350	0.247	0.234	0.172
Tb	0.7179	0.6324	0.245	0.232	0.172
Dy	0.7143	0.6313	0.244	0.231	0.172
Ho	0.7121	0.6293	0.243	0.229	0.171
Er	0.7100	0.6279	0.242	0.228	0.171
Yb	0.7044	0.6247	0.242	0.226	0.171

*$LaVO_4$ has a monzite structure with unit cell parameters $a = 0.707$ nm, $b = 0.729$ nm, $c = 0.677$ nm and $\beta = 105°$.

pores considerably reduce the conductivity, and measurements on them often do not reflect the bulk value for the material. It is not possible to eliminate these effects completely, but pellets can be prepared in such a way that they are considerably reduced, and in such a situation the bulk value for the material can be obtained by employing a suitable correction. The first requirement in this direction is to make pellets of uniform density. This has been achieved by using an appropriate steel die and keeping the ratio t^2/A (where t is the thickness and A the face area of the pellet) to less than four fixed by other workers [12].

Air pores are considerably reduced if these uniform pellets are made using fine-grain powders at a higher pelletizing pressure (P) and sintered at a higher temperature for longer times. Normally, pellets made at $P > 6 \times 10^8 \text{ N m}^{-2}$ have a density close enough ($\sim 80\%$) to the X-ray density of the material. The grain-boundary effect on pellets made at such a high pressure is considerably reduced. This fact is evident from the independency of a.c. electrical conductivity on signal frequency in the range 50 to 10^4 Hz. The electrodes used on the pellet faces also play a significant role in the σ and S measurements. For both measurements the stringent criterion [13] is to have ohmic contact between electrode and pellet interfaces. To investigate the nature of the contact, the d.c. current density (J) through the pellets was recorded as a function of applied electric field (E) for a platinum electrode. The plots (not shown) are almost linear right from $E = 0$ in a few cases, and above a certain value of E in all others. Thus contact between the pellet and the electrode interfaces is ohmic except at very low fields. In the measurement of σ at different temperatures, we have used well-sintered pellets made at higher pelletizing pressures ($P > 6 \times 10^8 \text{ N m}^{-2}$), keeping E in the range where contact between the pellet and the electrode faces was ohmic.

Both the Seebeck coefficient and the electrical conductivity of a few pellets of each compound were measured at different temperatures. Measurements of σ show a typical hysteresis around certain temperatures designated as T_3 and T_4. In the cooling part of a cycle, the peak observed at T_3 is normally reduced. However, at other temperatures the σ values are almost the same for heating and cooling. The Seebeck coefficient for each RVO_4 is essentially independent of the thermal history and shelf life of the pellet, and is reproducible to the extent of $\pm 5\%$. The results of σ and S measurements for light rare-earth vanadates have already been reported [6]. Figs 1 to 3 show the plots of $\log \sigma$ and S against T^{-1} for terbium,

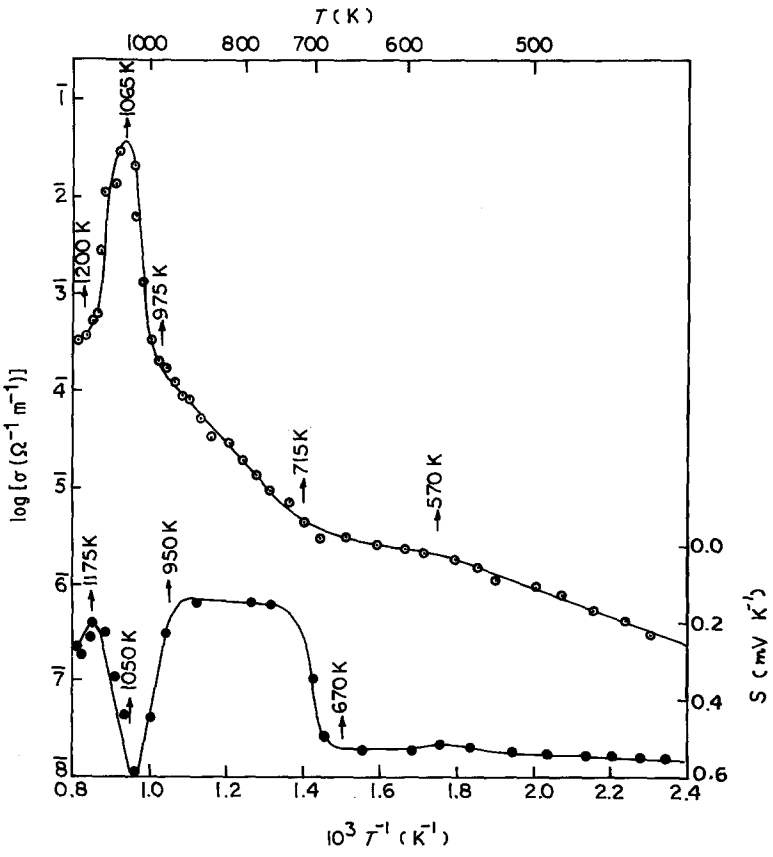

Figure 1 Plots of (⊙) logarithm of electrical conductivity ($\log \sigma$) and (●) Seebeck coefficient (S) against inverse of absolute tempeature (T^{-1}) for terbium vanadate.

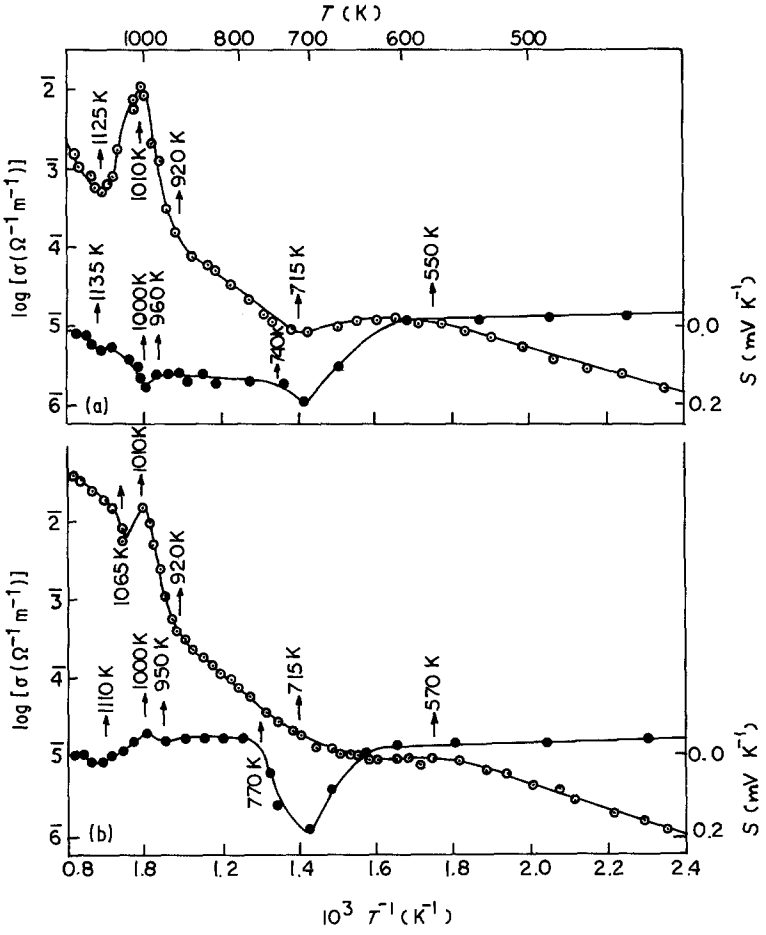

Figure 2 Plots of (⊙) logarithm of electrical conductivity ($\log\sigma$) and (●) Seebeck coefficient (S) against inverse of absolute temperature (T^{-1}) for (a) dysprosium and (b) holmium vanadates.

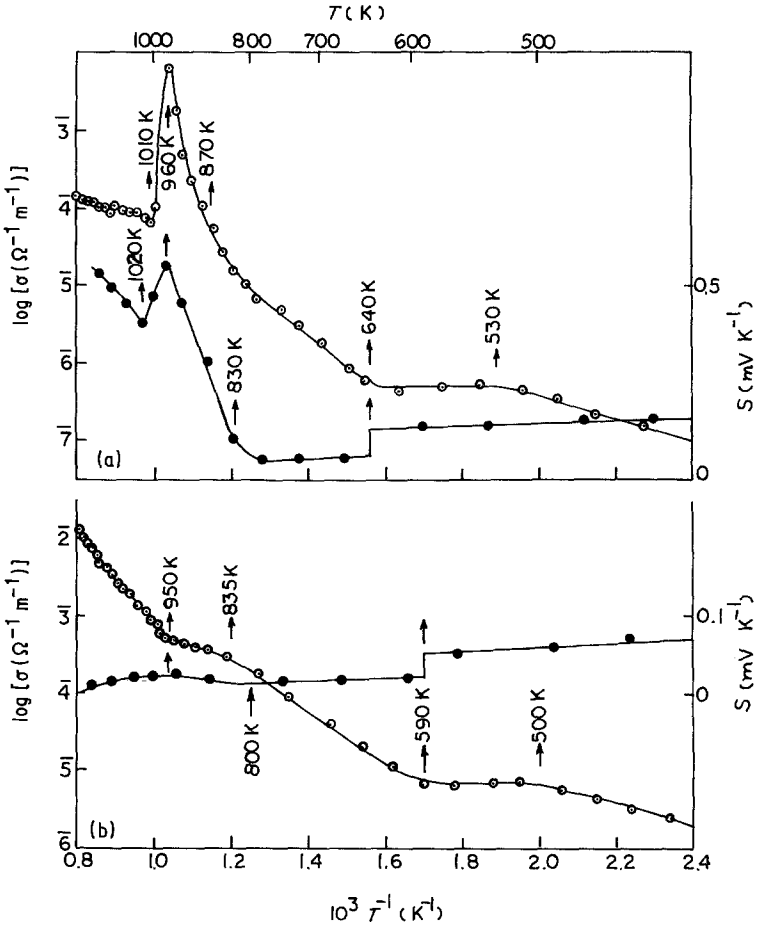

Figure 3 Plots of (⊙) logarithm of electrical conductivity ($\log\sigma$) and (●) Seebeck coefficient (S) against inverse of absolute temperature (T^{-1}) for (a) erbium and (b) ytterbium vanadates.

TABLE II Summarized results of electrical conductivity (σ) for RVO_4 below the break temperature T_2

R	σ at 500 K ($\Omega^{-1}m^{-1}$)	$T < T_1$			T_1 (K)	$T_1 < T < T_2$		
		σ_0 ($\Omega^{-1}m^{-1}$	E_a (eV)	T' (K)		σ_0 ($\Omega^{-1}m^{-1}$)	E_a (eV)	T_2 (K)
La	8.9×10^{-8}	–	–	–	435	1.05×10^{4}	0.84	840
Ce	1.9×10^{-2}	2.331	0.21	625	680	2.80×10^{3}	0.62	810
Pr	5.89×10^{-4}	0.096	0.22	625	660	2.08×10^{2}	0.64	800
Nd	3.02×10^{-4}	0.049	0.22	625	690	6.74×10^{1}	0.65	900
Sm	1.70×10^{-3}	0.984	0.20	625	690	3.44×10^{2}	0.66	900
Eu	5.75×10^{-3}	0.953	0.22	670	740	8.10×10^{2}	0.67	910
Gd	7.94×10^{-3}	1.097	0.22	555	745	3.25×10^{2}	0.68	920
Tb	8.71×10^{-7}	1.88×10^{-3}	0.30	570	715	1.93×10^{0}	0.80	975
Dy	5.37×10^{-6}	8.40×10^{-3}	0.29	570	715	1.42×10^{0}	0.75	920
Ho	4.78×10^{-6}	6.88×10^{-3}	0.29	570	715	7.69×10^{0}	0.80	920
Er	3.98×10^{-7}	8.40×10^{-3}	0.30	530	640	8.59×10^{-1}	0.79	870
Yb	6.31×10^{-6}	4.24×10^{-3}	0.25	500	590	4.70×10^{0}	0.69	835

dysprosium, holmium, erbium and ytterbium vanadates. The variations of σ and S with T^{-1} below T_1 (T_1' for S) can be represented by the general relations

$$\sigma = \sigma_0 \exp(-E_a/kT) \quad (1)$$

and

$$S = \frac{\eta}{eT} + H \quad (2)$$

where σ_0 and H are constants, E_a is the activation energy, k is Boltzmann's constant, e is the electronic charge and η is the slope of the S against T^{-1} line. The summarized results of σ and S together with the respective constants are given in Tables II and III, respectively. For generalization, data on light rare-earth vanadates have also been included.

Below T' K, σ values follow no sequence down the series of RVO_4. Above T', the long σ against T^{-1} plot becomes flat for all vanadates and remains so up to a temperature T_1. No time dependence was observed in J values at a fixed temperature. This indicates that charge carriers in these solids are electronic (i.e. either electrons or holes). Above T_1 the variations of $\log\sigma$ and S with T^{-1} are nearly linear and can be represented by Equations 1 and 2 with different values of the constants. Above T_2, these variations do not remain linear but yield a maximum around a temperature T_3 (T_3' for S), and then a minimum at T_4 ($T_4 > T_3$). Beyond T_4, the $\log\sigma$ against T^{-1} plot again increases with temperature. In $YbVO_4$, the σ variation remains linear and does not show any drop up to the highest temperature. The break temperatures T_1 and T_2 obtained from plots of $\log\sigma$ and S against T^{-1} are slightly different. This difference seems to be due to the different conditions in the measurements of σ and S. In the former, samples are kept in a uniform thermal state, whereas in the latter they are subjected to a thermal gradient. Thus in both cases the break temperatures reflect the same phenomenon in the sample.

4. Discussion

It has already been concluded that RVO_4 are essentially electronic semiconductors. The electronic conduction in semiconducting solids is usually explained using an energy band model. The relevant bands which may be important in the electrical conduction in these solids will be empty R^{3+} : 5d, V^{5+} : 4s and V^{5+} : 3d bands partially filled R^{3+} : $4f^n$ levels (or extremely narrow bands), and a completely filled O^{2-} : 2p band. The magnitude of the electrical conductivity in the studied RVO_4 is of the same order as that of V_2O_5 [14], and is several orders of magnitude larger than in the corresponding R_2O_3 [15, 16]. Thus the R^{3+} : 5d band should not come into the picture in the electrical conduction of these solids. The semi-empirical model proposed by Goodenough [17] is helpful in deciding the relative positions of these bands. Relevant optical

TABLE III Summarized results of Seebeck coefficient (S) for RVO_4 below the break temperature T_2

R	S at 500 K (mV K^{-1})	$T < T_1$				$T_1 < T < T_2$			
		Charge carrier	η (mV)	H (mV K^{-1})	T_1' (K)	Charge carrier	η (mV)	H (mV K^{-1})	T_2' (K)
La	+0.20	e	0.00	−0.230	430	e	+0.04	+0.18	670
Ce	−0.050	h	0.00	−0.050	680	h	−0.025	−0.048	810
Pr	−0.025	h	0.00	−0.025	660	h	−0.025	+0.003	770
Nd	+0.060	e	0.00	+0.060	690	e	+0.025	+0.007	900
Sm	+0.036	e	0.00	+0.036	690	e	+0.025	+0.025	835
Eu	+0.032	e	+0.008	+0.030	715	e	+0.002	+0.028	850
Gd	+0.043	e	+0.013	+0.038	600	e	+0.035	+0.021	890
Tb	−0.540	h	−0.05	−0.515	670	h	−0.05	−0.111	950
Dy	+0.050	e	+0.025	+0.037	740	h	−0.05	−0.241	960
Ho	+0.04	e	+0.025	+0.027	770	e	+0.05	+0.008	950
Er	+0.15	e	+0.025	+0.137	640	e	+0.025	+0.032	830
Yb	+0.06	e	+0.025	+0.047	590	e	+0.013	+0.012	800

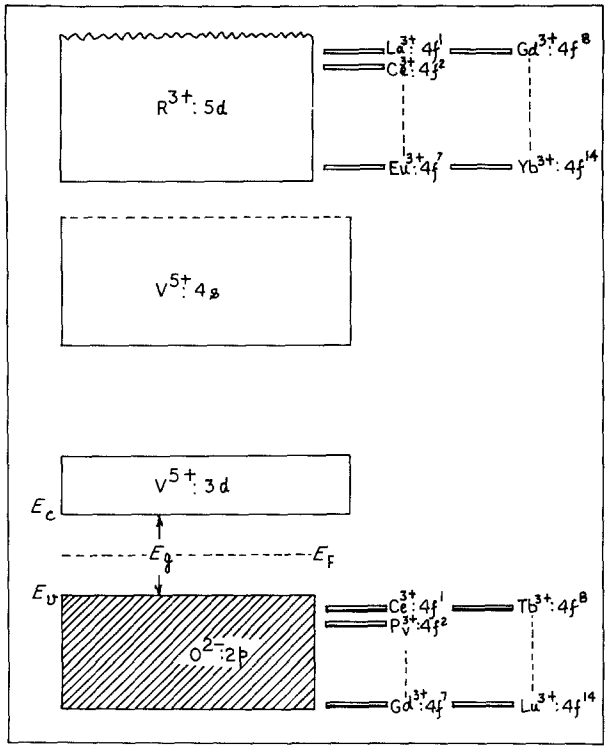

Figure 4 Schematic energy-band diagram for RVO_4.

data are not, however, available on these materials to apply it correctly. In any case the V^{5+} : 4s band should be separated from the V^{5+} : 3d band and should lie a few electron volts above it. RVO_4 are very stable and therefore the O^{2-} : 2p band should lie below V^{5+} : 3d band. The position of the R^{3+} : $4f^n$ levels is not very certain, but they must lie close to the top of the O^{2-} : 2p band. They will, however, shift sequentially down till they are half-filled ($4f^7$). These levels will go up again when the eighth electron enters the f level. However, they will then shift sequentially down and will lie in the lowest state for lutetium ($4f^{14}$). A general schematic energy-band diagram for RVO_4 will be as shown in Fig. 4. Based on this energy-band picture the intrinsic conduction in RVO_4 will occur by the following processes:

(i) Electrons from the filled O^{2-} : 2p band are excited to the empty V^{5+} : 3d band, leaving holes in the former. Thermally generated electrons in the V^{5+} : 3d (conduction) band and holes in the O^{2-} : 2p (valence) band will conduct in their respective bands. Both V^{5+} : 3d and O^{2-} : 2p bands will be narrow, and may split by the crystal field to make them still narrower. This will make the mobility of the charge carriers in both bands smaller.

(ii) In cases where $4f^n$ levels lie between the oxygen 2p and vanadium 3d bands, electrons may also be excited from $4f^n$ level to the V^{5+} : 3d band. In this case the dominant charge cariers will be electrons in the vanadium 3d band, as the holes created in $4f^n$ levels will be almost localized. The plot of $\log\sigma$ against T^{-1} will also be linear with a slope corresponding to an energy of $W/2$, where W is the difference of energy between the $4f^n$ level and the bottom of the V^{5+} : 3d band. However, if this is true, the linear variation of S against T^{-1} should also yield a slope corresponding to an energy of $W/2$ [18]. This is not true, as the experimentally observed slope of the S against T^{-1} plot is almost zero in all cases. This means that mechanism (ii) of intrinsic conduction is not effective and $4f^n$ levels lie below the top of the oxygen 2p band. Thus intrinsic band conduction, as described in (i) above, is the dominant conduction mechanism in these solids. The solid may have electrons or holes as the dominant charge carriers, depending upon the values of electron or hole mobility (μ_e and μ_h) and their effective masses (m_e^* and m_h^*) in the respective bands.

At higher temperatures ($T > T_2$) the process described in (i) may be the mechanism of electrical conduction in these solids. The variations of σ and S in the case of the two-band model will be the same as given in our previous paper [6]. Adopting the same procedure as in the above-mentioned paper, we can evaluate the ratios of the effective masses of electrons in the conduction band and holes in the valence band ($a = m_e^*/m_h^*$) as well as their mobilities. These evaluated values are given in Table IV. It is seen from this table that the mobilities of the majority charge carriers lie in the range 10^{-11} to $10^{-7}\,m^2\,V^{-1}\,sec^{-1}$, which are orders of magnitude smaller than one expects in normal band conduction [19]. The prime reason of this seems to be polaron formation [20, 21]. The mobility in this case becomes very small and is thermally activated. The activation energy in this case becomes $(E_g - 2\hbar\omega_0)/2$ where ω_0 is the longitudinal optical mode frequency, which will be of the order of 10^{14} Hz.

TABLE IV Properties of charge carriers in RVO_4

R	Energy band gap E_g (eV)	Ratio of mobilities	Ratio of effective mass	Mobility at 800 K	
				$\mu_e \times 10^9$ ($m^2\,V^{-1}\,sec^{-1}$)	$\mu_h \times 10^9$ ($m^2\,V^{-1}\,sec^{-1}$)
La	1.68	1.10	1.956×10^2	6.03	5.48
Ce	1.24	0.922	0.144	329	357
Pr	1.28	0.925	1.162	5.12	5.54
Nd	1.30	1.080	1.006	1.99	1.85
Sm	1.32	1.079	1.330	8.27	7.66
Eu	1.34	1.006	1.529	16.94	16.84
Gd	1.36	1.109	1.206	8.51	7.68
Tb	1.60	0.882	0.016	1.17	1.33
Dy	1.50	0.875	1.571×10^{-4}	27.10	30.97
Ho	1.60	1.065	2.114×10^{-2}	4.11	3.86
Er	1.58	1.065	1.508	0.019	0.018
Yb	1.38	1.038	1.146	0.124	0.120

TABLE V Electrical conductivity data for RVO_4

R	T_3-T_2 (K)	T_3 (K)	T_4 (K)	$\sigma(T_2)$ ($\Omega^{-1}m^{-1}$)	$\sigma(T_3)$ ($\Omega^{-1}m^{-1}$)	$\frac{\sigma(T_3)}{\sigma(T_2)}$	$\sigma(T_4)$ ($\Omega^{-1}m^{-1}$)
La	30	870	–	1.53×10^{-4}	7.08	5.0×10^4	–
Ce	90	900	1090	0.365	4.79	13.2	5.25×10^{-2}
Pr	100	900	1100	0.027	0.28	10.4	3.98×10^{-4}
Nd	90	990	1110	0.016	0.16	10.0	3.80×10^{-4}
Sm	90	990	1120	0.063	0.25	4.0	2.29×10^{-4}
Eu	90	1000	1125	0.151	0.48	3.2	9.77×10^{-4}
Gd	80	1000	1130	0.078	0.22	2.8	9.10×10^{-5}
Tb	90	1065	1200	1.78×10^{-4}	0.037	209	3.31×10^{-4}
Dy	90	1010	1125	1.23×10^{-4}	0.011	91.0	6.03×10^{-4}
Ho	90	1010	1065	3.89×10^{-4}	0.018	45.8	6.61×10^{-3}
Er	90	960	1010	4.07×10^{-5}	0.006	145	6.30×10^{-5}

Thus the band gap given Table IV should be increased by this amount (~ 0.13 eV).

The electrical conductivity of all vanadates increases at a much faster rate above T_2. It gives a maximum at T_3 and then drops sharply (except in ytterbium vanadate), shows a minimum around T_4 and then increases with increase of temperature. Table V shows the temperature span ($T_3 - T_2$), σ at T_2, T_3 and T_4 and the ratio of values at T_2 and T_3. For the sake of comparison and discussion, we have included the data on $LaVO_4$ [5] and light rare-earth vanadates [6] published earlier. It is worth mentioning that in $LaVO_4$ the electrical conductivity jumps by a factor of 5×10^4 within a temperature span of 30 K. This jump has been recognized by us [5] as a semiconductor–semimetal transition occurring due to the approach and finally the overlap of valence and the conduction bands. This tendency of the energy band gap to decrease with temperature continues in other members of RVO_4. This is the reason for the increase of σ in all vanadates at a much faster rate above T_2. All rare-earth vanadates tend to become semimetal at higher temperatures. However, up to T_3 they only achieve a conductivity which is an order of magnitude less than the value one expects for a good semimetal. The ratio $\sigma(T_3)/\sigma(T_2)$ decreases as we go down the series from lanthanum to gadolinium, but becomes large for terbium and continues to increase as we go further down in the series.

The decrease of σ above T_3 and the appearance of a minimum in the $\log \sigma$ against T^{-1} plot around T_4 for all vanadates seems to be due to a phase transition. The DTA plot (Fig. 5) shows a big flat dip in the temperature interval 1075 to 1300 K for different vanadates. We believe that rare-earth vanadates undergo a phase transition within the above-mentioned temperature interval. The minimum observed around T_4 in the $\log \sigma$ against T^{-1} plots for different vanadates lies well within the above temperature range, and can be termed the phase transition temperature. It is worth mentioning at this stage that all vanadates (except the lanthanum one) at room temperature have a tetragonal zircon-type structure. Such structures have a tendency to change to the scheelite structure [22]. We believe that the phase transition around T_4 is a transformation in rare-earth vanadates from a low-temperature zircon to a high-temperature scheelite structure.

Below T_1' the activation energy E_a is small for all vanadates. Such a low activation energy cannot be due to intrinsic band conduction. It is seen from Figs 1 to 3 that S remains paractically constant in all vanadates below T_1'. This indicates that the charge carriers are not thermally generated, and that their number remains practically constant in this temperature range. This may happen when charge carriers are localized on defect centres and they conduct via a hopping mechanism. It is worth mentioning in this respect that the presence of V^{4+} defect centres in RVO_4 has been indicated by our magnetic susceptibility studies [2–4]. These centres are created due to oxygen deficiencies in these materials. These centres

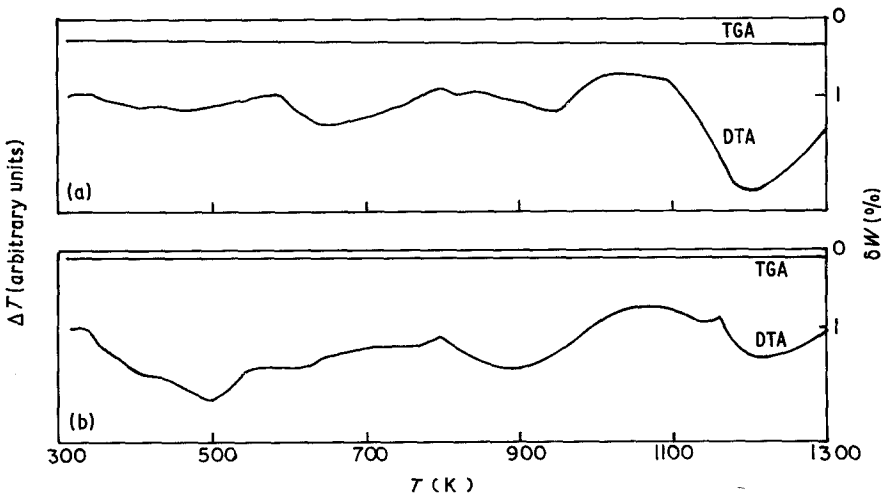

Figure 5 TGA and DTA plots for (a) gadolinium and (b) ytterbium vanadates.

TABLE VI Concentrations of normal sites and defect centres in RVO_4, and resulting Seebeck coefficient and hopping mobility of the charge carriers

R	Concentration of normal sites, $N \times 10^{-28}$ (m^{-3})	Concentration of defect centres, n (m^{-3})	Calculated Seebeck coefficient, S ($mV\,K^{-1}$)	Hopping mobility at 500 K ($m^2\,V^{-1}\,sec^{-1}$)
La	–	–	–	–
Ce	1.13	6.76×10^{23}	0.84	1.77×10^{-6}
Pr	1.14	1.32×10^{22}	1.20	2.79×10^{-6}
Nd	1.16	8.64×10^{21}	1.22	2.19×10^{-6}
Sm	1.19	3.92×10^{22}	1.09	2.72×10^{-6}
Eu	1.20	1.69×10^{23}	0.96	2.58×10^{-6}
Gd	1.21	2.95×10^{23}	0.92	2.28×10^{-6}
Tb	1.23	1.04×10^{20}	1.60	1.64×10^{-7}
Dy	1.24	5.14×10^{21}	1.27	1.17×10^{-6}
Ho	1.25	4.60×10^{20}	1.48	1.16×10^{-6}
Er	1.26	4.86×10^{19}	1.67	9.17×10^{-7}
Yb	1.29	2.45×10^{20}	1.53	2.88×10^{-6}

can also play a significant role in conduction, and in the lower temperature range the electrons from V^{4+} defect centres can hop to V^{5+} normal sites. We expect this to be the predominant conduction mechanism in most of the vanadates below T_1'. The charge carriers in this process will be electrons. However, the dominant charge carriers in this temperature range for cerium, praseodymium and terbium vanadates are holes rather than electrons. This means that there are very few V^{4+} centres in these vanadates. This may arise because V^{4+} centres are formed due to oxygen deficiency in RVO_4. These vanadates are prepared using the following solid-state reactions:

$$4CeO_2 + 2V_2O_5 \rightarrow 4CeVO_4 + O_2$$

$$Pr_6O_{11} + 3V_2O_5 \rightarrow 6PrVO_4 + O_2$$

$$2Tb_4O_7 + 4V_2O_5 \rightarrow 8TbVO_4 + O_2$$

In view of the above equations, oxygen deficiency and thus the existence of V^{4+} centres is not expected in cerium, praseodymium and terbium vanadates. However, all these elements have more tendency to be present in their respective solids as tetravalent (Ce^{4+}, Pr^{4+} and Tb^{4+}) ions rather than the usual trivalent (Ce^{3+}, Pr^{3+} and Tb^{3+}) ions common to other rare earths. CeO_2, Pr_6O_{11} and Tb_4O_7 are the most stable oxides of cerium, praseodymium and terbium, respectively. Thus the existence of Ce^{4+} centres in cerium, Pr^{4+} centres in praseodymium and Tb^{4+} centres in terbium vanadates are quite possible. They can take part in conduction as a hole from these (Ce^{4+}, Pr^{4+} and Tb^{4+}) defect centres can hop to trivalent (Ce^{3+}, Pr^{3+} and Tb^{3+}) normal sites. This is probably the dominant conduction mechanism in such vanadates below T'.

The Seebeck coefficient in the case of hopping conduction is given by Heike's formula [23]. Using this relation we have evaluated the S values for all vanadates using the procedure explained elsewhere [9, 11]. The calculated values are given in Table VI. It is seen from this table that the observed values of S are much smaller compared with the values one expects from the conduction of electrons or holes on defect centres. This indicates that both types of defect centre (one capable of giving holes and the other electrons) do exist in all rare-earth vanadates. In some vanadates the slope of the $\log\sigma$ against T^{-1} plot becomes very small above T', and in a few the curve almost becomes flat. This lowering of activation energy is probably brought about by the reduction of the potential barrier between V^{4+} and V^{5+} due to the presence of some electrons in the excited state of V^{4+} sites. In the case of hole conductors this reduction is brought about by the presence of holes in thermally excited states of R^{4+} centres. However, the flattening of the $\log\sigma$ against T^{-1} plot is probably due to the smoothing of the potential barrier by thermal fluctuations, leading to the freeing of electrons (or holes) in increasing numbers at higher temperatures.

Acknowledgements

The financial assistance given by CSIR, India for this work in the form of a Senior Research Fellowship to one of us (K.G.) is thankfully acknowledged. The authors are also grateful to Dr D. C. Agrawal, Department of Materials Science, IIT Kanpur for DTA and TGA studies.

References

1. G. A. GEHRING and K. A. GEHRING, *Rep. Prog. Phys.* **38** (1975) 1.
2. KANCHAN GAUR, A. K. TRIPATHI and H. B. LAL, *J. Mater. Sci. Lett.* **2** (1983) 161.
3. *Idem, ibid.* **2** (1983) 371.
4. KANCHAN GAUR and H. B. LAL, *ibid.* **2** (1983) 744.
5. *Idem, J. Mater. Sci.* **19** (1984) 3325.
6. *Idem, ibid.* **20** (1985) 3167.
7. R. W. G. WYCKOFF, *Cryst. Struct.* **3** (1965) 17.
8. A. K. TRIPATHI, PhD thesis, Gorakhpur University (1981).
9. A. K. TRIPATHI and H. B. LAL, *J. Mater. Sci.* **17** (1982) 1595.
10. H. B. LAL, B. K. VERMA and V. R. YADAV, *ibid.* **17** (1982) 3317.
11. KANCHAN GAUR, PhD thesis, University of Gorakhpur (1984).
12. R. KUMAR, *Science Reporter* **8** (1971) 568.
13. G. G. ROBERTS, "Transfer and storage of energy in molecules", edited by G. M. Burnett, A. N. North and J. N. Sherwood, Vol. 4 (Wiley, London, 1974) p. 153.
14. N. F. MOTT, "Metal–Insulator Transitions" (Taylor and Francis, London, 1974) p. 160.

15. A. KUMAR, PhD thesis, University of Gorakhpur (1975).
16. H. B. LAL, B. K. VERMA and N. DAR, *Indian J. Cryo.* **1** (1976) 119.
17. G. B. GOODENOUGH, *J. Appl. Phys.* **37** (1966) 1415.
18. T. C. HERMAN and J. M. HONIG, "Thermoelectric and thermomagnetic effects and applications" (McGraw-Hill, New York, 1967) p. 142.
19. J. APPEL, *Solid State Phys.* **21** (1968) 193.
20. I. G. AUSTIN and N. F. MOTT, *Adv. Phys.* **18** (1969) 41.
21. A. J. BOSMAN and H. J. VAN DAAL, *ibid.* **19** (1970) 1.
22. V. S. STUBICAN and R. ROY, *Z. Kristallogr.* **119** (1963) 90.
23. R. R. HEIKES and R. W. URS (editors), "Thermoelectricity, Science and Engineering" (Interscience, New York, 1961). 45.

Received 28 March
and accepted 10 September 1985